Cell Research (2011) 21:817-834.

www.nature.com/cr

ORIGINAL ARTICLE

Mitochondrial H_2O_2 generated from electron transport chain complex I stimulates muscle differentiation

Seonmin Lee[1], Eunyoung Tak[1], Jisun Lee[1], MA Rashid[1], Michael P Murphy[2], Joohun Ha[1], Sung Soo Kim[1]

[1]*Department of Biochemistry and Molecular Biology, Medical Science and Engineering Research Center for Bioreaction to Reactive Oxygen Species and Biomedical Science Institute (BK-21), School of Medicine, Kyung Hee University, #1, Hoegi-dong, Dongdaemoon-gu, Seoul 130-701, Korea;* [2]*MRC Mitochondrial Biology Unit, Hills Road, Cambridge CB2 0XY, UK*

Mitochondrial reactive oxygen species (mROS) have been considered detrimental to cells. However, their physiological roles as signaling mediators have not been thoroughly explored. Here, we investigated whether mROS generated from mitochondrial electron transport chain (mETC) complex I stimulated muscle differentiation. Our results showed that the quantity of mROS was increased and that manganese superoxide dismutase (MnSOD) was induced via NF-κB activation during muscle differentiation. Mitochondria-targeted antioxidants (MitoQ and MitoTEMPOL) and mitochondria-targeted catalase decreased mROS quantity and suppressed muscle differentiation without affecting the amount of ATP. Mitochondrial alterations, including the induction of mitochondrial transcription factor A and an increase in the number and size of mitochondria, and functional activations were observed during muscle differentiation. In particular, increased expression levels of mETC complex I subunits and a higher activity of complex I than other complexes were observed. Rotenone, an inhibitor of mETC complex I, decreased the mitochondrial NADH/NAD^+ ratio and mROS levels during muscle differentiation. The inhibition of complex I using small interfering RNAs and rotenone reduced mROS levels, suppressed muscle differentiation, and depleted ATP levels with a concomitant increase in glycolysis. From these results, we conclude that complex I-derived $O_2\cdot^-$, produced through reverse electron transport due to enhanced metabolism and a high activity of complex I, was dismutated into H_2O_2 by MnSOD induced via NF-κB activation and that the dismutated mH_2O_2 stimulated muscle differentiation as a signaling messenger.

***Keywords*:** mitochondria; mitochondrial electron transport chain; ROS; MnSOD; muscle differentiation
Cell Research (2011) **21**:817-834. doi:10.1038/cr.2011.55; published online 29 March 2011

Introduction

Mitochondria are primary producers of energy in the form of ATP via oxidative phosphorylation, employing a series of electron flow processes through an electron transport chain (ETC) [1, 2]. The mitochondrial ETC consists of four multi-subunit complexes (complexes I-IV), which, along with the F_0F_1-ATP synthase (complex V), are encoded by either mitochondrial or nuclear DNA [3].

Mitochondrial reactive oxygen species (mROS) are formed as by-products of the mitochondrial ETC (mETC) during the generation of ATP or by an imbalance in cellular oxidant/antioxidant systems [4, 5]. Among the mETC complexes, complexes I and III are considered major generating sites of superoxide ($O_2\cdot^-$). Complex I generates $O_2\cdot^-$ within the mitochondrial matrix only, whereas complex III generates $O_2\cdot^-$ in the intermembrane space and in the matrix [6]. Many reports have shown that mROS are frequently implicated in a wide range of pathological conditions, including cancers, atherosclerosis, diabetes, neurodegenerative diseases, and aging [3, 7-10]. However, recent studies have suggested that mROS also play important physiological functions, such as the induction of nutrient sensing within the hypothalamus [11] and the prevention of TNF-induced apoptosis by enhancing the NF-κB-mediated expression of anti-apoptotic proteins [12].

Correspondence: Sung Soo Kim
Tel: 82-2-961-0524; Fax: 82-2-959-8168
E-mail: sgskim@khu.ac.kr
Received 11 Mar 2010; revised 2 August 2010; accepted 20 October 2010; published online 29 March 2011

ROS include $O_2\cdot^-$, hydroxyl radicals ($OH\cdot^-$), and hydrogen peroxide (H_2O_2) [13]. H_2O_2 is the only ROS that can function directly as a second messenger in a physiologically relevant manner [14]. Manganese superoxide dismutase (MnSOD) is the first anti-oxidant enzyme in the mitochondrial matrix and is encoded by the nuclear SOD2 gene. MnSOD catalyzes the dismutation of $O_2\cdot^-$ to H_2O_2 [15]. Therefore, MnSOD is not only a critical cytoprotector against oxidative stress but also a mediator of mitochondrial ROS signaling through the generation of H_2O_2, which is membrane permeable [16].

Muscle differentiation is a multi-step process that involves the expression of muscle regulatory factors, cell cycle arrest, myoblast elongation, and cell fusion into multinuclear myotubes. Each of these stages is regulated by two groups of myogenic transcription factors, the myocyte enhancer binding factor 2 proteins A-D and the myogenic regulatory factors (MRFs), including Myf5, MyoD, Myogenin, and MRF4. Insulin and IGF-I and -II are the best-characterized ligands for muscle differentiation. The role of diverse signaling molecules in muscle differentiation, including phosphatidylinositol 3-kinase, Akt, Rac, $p70^{S6K}$, phospholipase C-β1 and γ1, the mammalian target of rapamycin and p38 MAPK, has been well established [17, 18].

H_2O_2 originating from NADPH oxidase has been considered an essential mediator for the differentiation of diverse cells, including embryonic cardiomyogenesis [19]. We have also previously reported that NADPH oxidase is actively involved in muscle differentiation [20]. Here, we focused on mitochondria as another ROS source for muscle differentiation and found that H_2O_2 generated from mETC complex I stimulates muscle differentiation.

Results

Generation of mitochondrial ROS increases during muscle differentiation

We first examined whether mitochondria generated ROS during muscle differentiation. Our H9c2 myoblasts differentiated well, as shown in Figure 1A. We detected ROS in mitochondria via confocal microscopy using the mitochondrial superoxide indicator MitoSOX. To visualize the nuclei and the mitochondria, we stained the cells using Hoechst 33342 and $DiOC_6$, respectively. As shown in Figure 1B, MitoSOX co-localized with $DiOC_6$. Compared with the proliferative stage, $O_2\cdot^-$ was increased in mitochondria during differentiation. In addition, mitochondrial H_2O_2 (mH_2O_2) levels were two-fold higher in the mitochondria isolated from DM stage cells than those from PM stage cells (Figure 1C). Finally, we tested whether MnSOD, the primary antioxidant enzyme in the mitochondrial matrix for neutralizing $O_2\cdot^-$, was induced during differentiation because its induction has been shown to be an indicator for mitochondrial ROS (mROS) generation [21]. The expression level of MnSOD in the mitochondrial fraction was increased (Figure 1D). VDAC was used to verify that mitochondrial proteins were equally loaded for western blotting. From these results, we hypothesized that increased mitochondrial $O_2\cdot^-$ induced MnSOD expression and that the induced MnSOD rapidly dismutated $O_2\cdot^-$ into H_2O_2, which stimulated muscle differentiation after diffusing from the mitochondria into the cytosol.

MnSOD is transcriptionally induced via NF-κB activation during myogenic differentiation

Because MnSOD was induced during muscle differentiation (Figure 1D), we further tested whether MnSOD induction increased in a time-dependent manner. The results showed that this was indeed the case (Figure 2A). Next, we assessed whether MnSOD expression was transcriptionally regulated during muscle differentiation via semiquantitative reverse transcriptase-polymerase chain reaction (RT-PCR) (Figure 2B) and real-time quantitative RT-PCR (Figure 2C) analysis. Both results showed that MnSOD mRNA levels were increased during differentiation. To exclude the possibility of mRNA stabilization, we treated the differentiating cells with 5 μg/ml actinomycin D, which inhibits *de novo* mRNA synthesis, for the indicated periods of time and then assessed the level of MnSOD mRNA. The results revealed that MnSOD mRNA disappeared almost completely 8 h after actinomycin D treatment (Figure 2D, top). We further assessed the decay rate of the mRNA via treatment with actinomycin D in PM and DM for up to 24 h after induction in DM for 24 hours. As shown in Figure 2D (bottom), the decay rate of MnSOD mRNA was similar in both PM and DM, indicating that transcriptional activation is involved in MnSOD induction during muscle differentiation. In a previous study, MnSOD was shown to be transcriptionally regulated by the intracellular redox balance-related transcription factor NF-κB [4]. To determine whether NF-κB regulated MnSOD transcription in our system, we investigated the translocation of NF-κB from the cytosol to the nucleus during differentiation. As shown in Figure 2E, NF-κB translocated to the nucleus during differentiation. Phospho-IκB in the cytoplasm was also increased during differentiation without any variation in total IκB levels. To investigate whether the MnSOD promoter had the consensus NF-κB binding sequence 5′-GGGPuNNPyPyCC-3′, we investigated the rat SOD2 promoter using bioinformatics analysis. We identified three putative NF-κB-binding sequences located

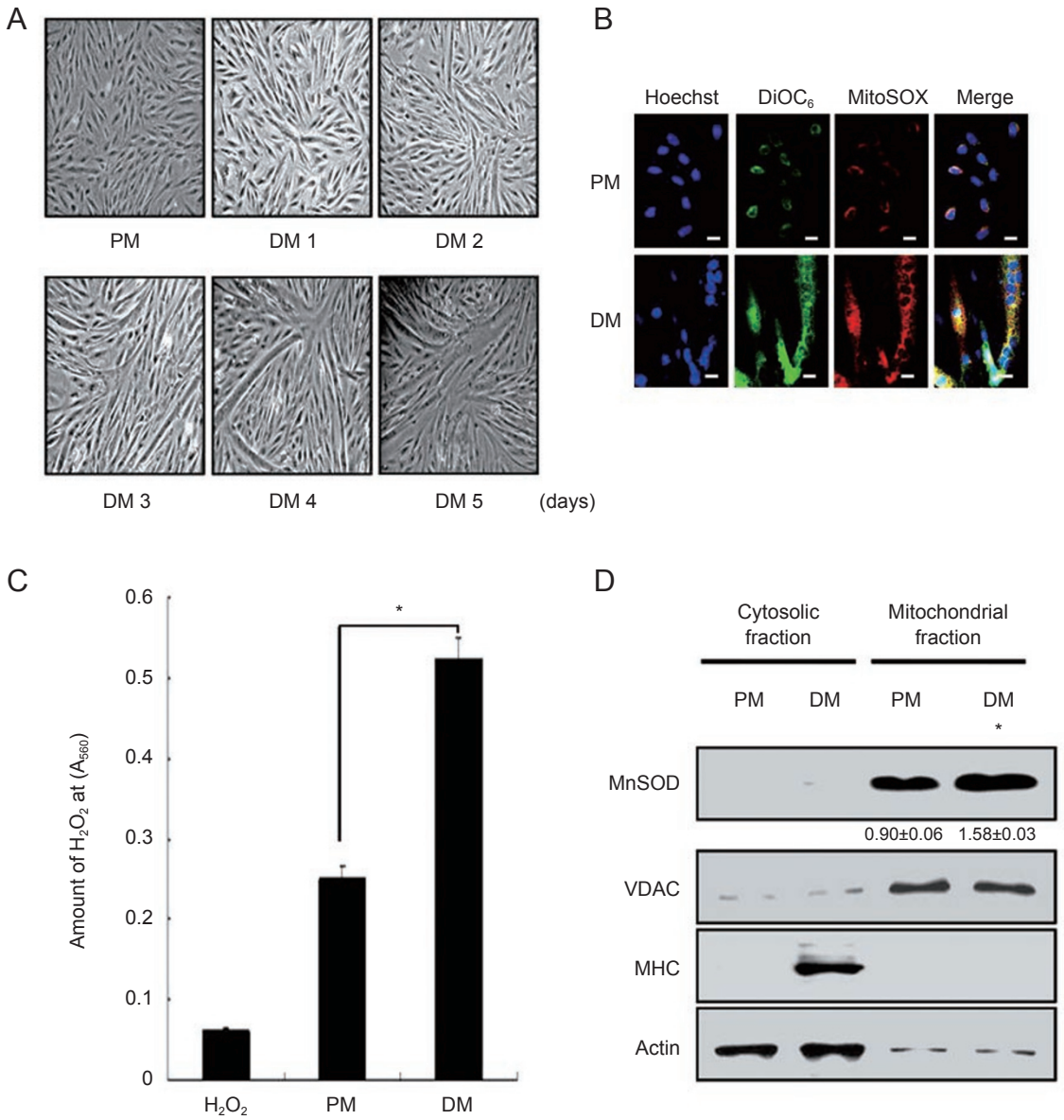

Figure 1 Increase in mitochondrial ROS generation during muscle differentiation. **(A)** Morphological changes with progression of differentiation in DM for up to 5 days. **(B)** Enhanced mROS generation was verified via confocal microscopy. Mitochondria tracker $DiOC_6$, green; mitochondrial ROS indicator MitoSOX, red; nuclear indicator Hoechst 33342, blue. Scale bar, 20 μm. **(C)** H_2O_2 in isolated mitochondria. The level of H_2O_2 was measured using Amplex Red. A total of 1 mM H_2O_2 was used as a standard control. Data represent mean ± SE, n = 3. *P < 0.001 vs PM. **(D)** Expression levels of MnSOD and MHC were analyzed using western blot. The MnSOD expression level was quantified using scanning densitometry (Quantify One—4.6.2 Basic). Data represent means ± SE, n = 3. *P < 0.001 vs PM. VDAC and actin were used as loading controls.

–430, –960 and –1 000 bp upstream of the SOD2 start codon (Figure 2F). Then, to investigate the binding activity of NF-κB to the MnSOD promoter, we constructed reporter plasmids, transiently transfected them into H9c2 cells, and then monitored luciferase activity during differentiation. Luciferase activity was only induced in a construct harboring the full-length MnSOD upstream element during differentiation. This result indicated that one of the two regions located at −960 or −1 000 bp may be involved in the induction of MnSOD transcription (Figure 2G, left). For further investigation, we conducted mutagenesis studies using the pGL3-SOD2/1023 luciferase plasmid. The luciferase activity of the mutant within the NF-κB binding site at –960 bp was dramati-

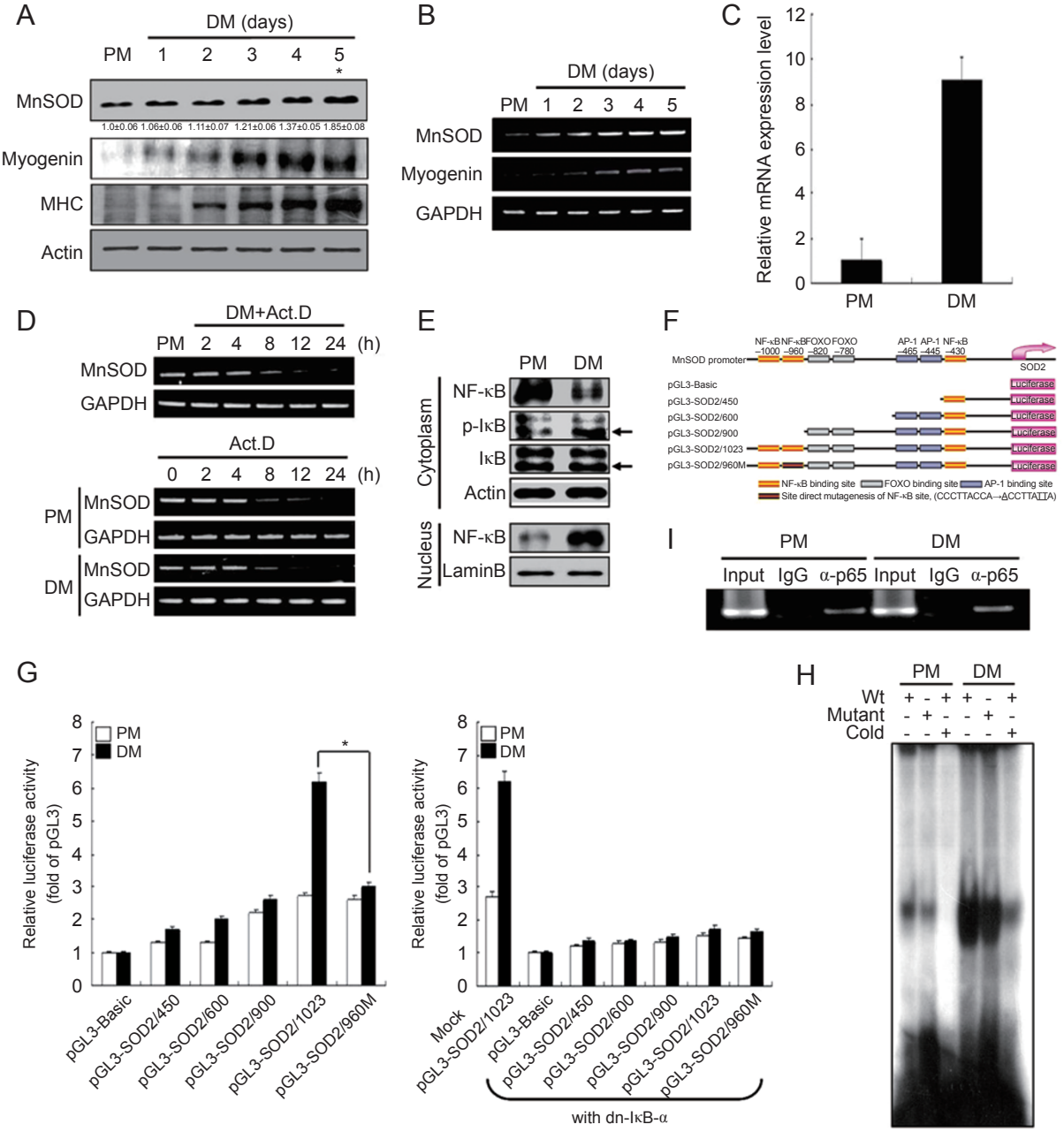

Figure 2 Induction of MnSOD via NF-κB during myogenesis. **(A)** Both MnSOD and MHC were analyzed using western blotting using specific antibodies. Protein levels were standardized against actin. The MnSOD expression level was quantified using scanning densitometry (Quantify One—4.6.2 Basic). Data represent means ± SE, n = 3. *P < 0.001 vs PM. **(B)** MnSOD and myogenin mRNA levels were analyzed using RT-PCR. GAPDH mRNA was used as an internal control. **(C)** Real-time quantitative RT-PCR analysis for MnSOD mRNA. **(D)** Transcriptional regulation of MnSOD expression. Confluent cells in PM were further exposed to DM with actinomycin D (5 μg/ml) for the indicated time periods, and semiquantitative RT-PCR analysis was conducted (top). Cells incubated in DM for 24 h were again exposed to PM and DM with actinomycin D, and mRNA levels of MnSOD were determined using semiquantitative RT-PCR analysis (bottom). **(E)** Translocation of NF-κB to the nucleus. NF-κB was determined in paired cytoplasmic and nuclear fractions using western blotting with specific antibodies. Lamin B was used as a nuclear protein marker. **(F)** MnSOD promoter analysis. Putative NF-κB binding sites in the MnSOD promoter were analyzed up to 1 023 bp upstream of the MnSOD transcriptional initiation site. Deleted and site-directed mutagenized constructs at the putative NF-κB-binding site were constructed for the luciferase reporter assay. **(G)** Luciferase reporter assay. Data represent means ± SE, n = 3. *P < 0.001 vs pGL3-SOD2/1023 in DM. **(H)** EMSA. **(I)** ChIP assay. The NF-κB binding site within the –960 region was analyzed using antibodies against the p65 subunit of NF-κB. Input genomic DNA (input) was used as a positive control and immunoprecipitation using nonspecific IgG (IgG) was used as a negative control.

cally decreased (Figure 2G, left), while the luciferase activity of the mutant within the NF-κB binding site at –1 000 bp did not change (data not shown). Therefore, we concluded that the region within –960 bp is indispensable for the induction of MnSOD mRNA. To further determine the involvement of NF-κB in the induction of MnSOD mRNA, we cotransfected the luciferase reporter constructs with a dominant-negative IκB-α (S32/36A, dn-IκB-α) construct, which suppresses proteasome-dependent degradation of phosphorylated IκB-α and, thereby, NF-κB translocation [22]. As shown in Figure 2G (right), the luciferase activity did not change, even in constructs harboring the full-length MnSOD upstream element. In our study, AP-1 and FOXO binding sites were not involved in MnSOD transcription. Previously, it was reported that AP-1 and FOXO are involved in myogenic differentiation [23]. However, other studies have reported that they are negatively associated with myogenesis in a

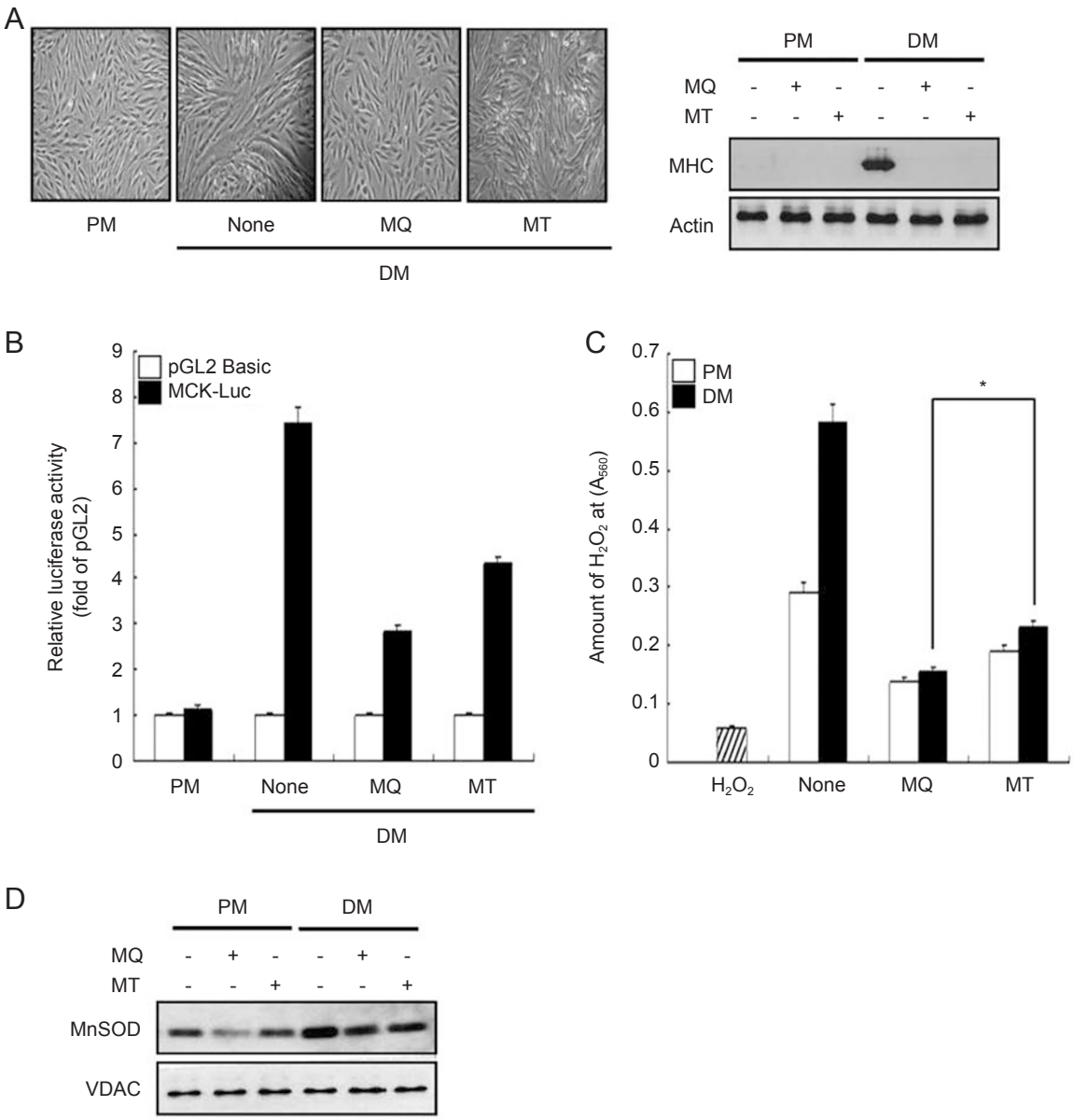

Figure 3 Elimination of mitochondrial ROS impairs muscle differentiation. Cells were induced to differentiate for 5 days in DM with or without MitoQ (MQ, 200 nM) and MitoTEMPOL (MT, 100 μM). **(A)** Morphological changes and expression level of MHC. **(B)** MCK-dependent luciferase assay (MCK-Luc). **(C)** H_2O_2 level in isolated mitochondria. A total of 1 mM H_2O_2 was used as a standard control. Data represent means ± SE, $n = 3$. *$P < 0.001$ vs absence of drug in DM. **(D)** Effect of MitoQ and MitoTEMPOL on the expression levels of MnSOD and MHC. VDAC was used as a mitochondrial protein marker.

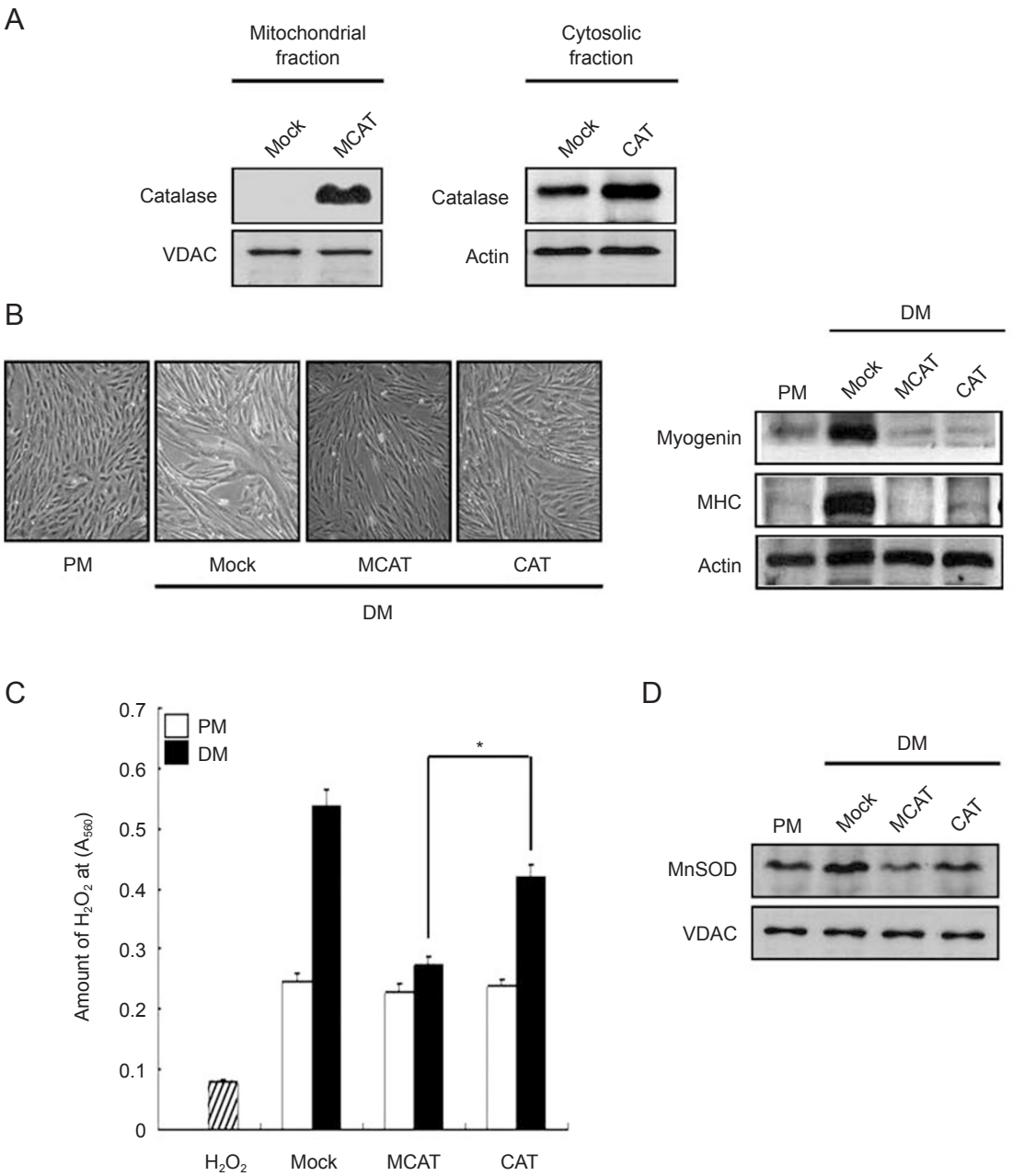

Figure 4 Effect of mitochondria-targeted catalase on muscle differentiation. Cells were transduced with rAd.lacZ, rAD.CMVM-CAT (MCAT), and rAd.CMVCAT (CAT) at an MOI of 200 in DM for 5 days. **(A)** Determination of recombinant viral transduction efficiency using western blot. **(B)** Inhibitory effect of MCAT and CAT on muscle differentiation. **(C)** H_2O_2 levels in isolated mitochondria. A total of 1 mM H_2O_2 was used as a standard control. Data represent mean ± SE, n = 3. *P < 0.001 vs mock cells in DM. **(D)** Expression level of MnSOD.

C2C12 model [24]**.** Electrophoretic mobility shift assay (EMSA) analysis was performed using ^{32}P-labeled wild-type NF-κB or mutated oligonucleotide probes. In DM, the wild-type oligonucleotides showed stronger binding than the mutated oligonucleotides (Figure 2H). The binding was abolished by a hundred-fold excess amount of unlabeled competitor oligonucleotides. Chromatin immunoprecipitation (ChIP) assays also showed that the NF-κB binding sequence of the MnSOD promoter was associated with NF-κB (Figure 2I).

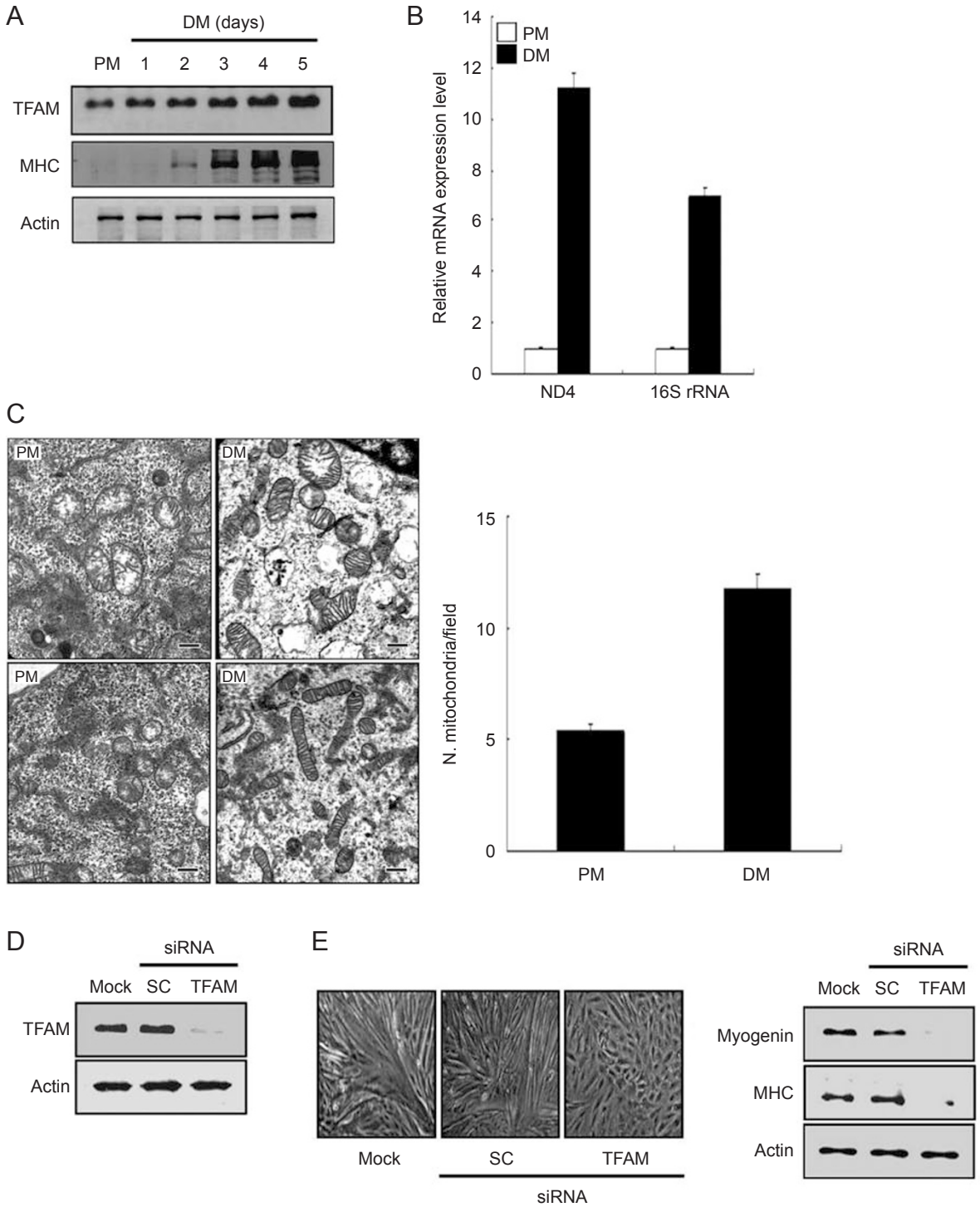

Figure 5 Mitochondrial alterations by induced TFAM during muscle differentiation. Cells were induced to differentiate for the indicated time periods in DM. **(A)** Expression levels of TFAM. **(B)** Real-time quantitative RT-PCR analysis for transcripts of mtDNA-encoded genes. **(C)** Ultrastructural features of mitochondria. Transmission electron microscopy analysis. Left, mitochondria in PM-stage cell; middle, mitochondria in DM-stage cell; right, statistical analysis of mitochondria from chosen fields in PM and DM. The original magnification was 12 000× and scale bars indicate 0.6 μm. Two typical morphologies are shown. **(D)** Knockdown of TFAM using siRNA. **(E)** Differentiation was blocked by knockdown of TFAM using specific siRNA. Scrambled control siRNA (SC) was used as a control for this study. Actin was used as a loading control.

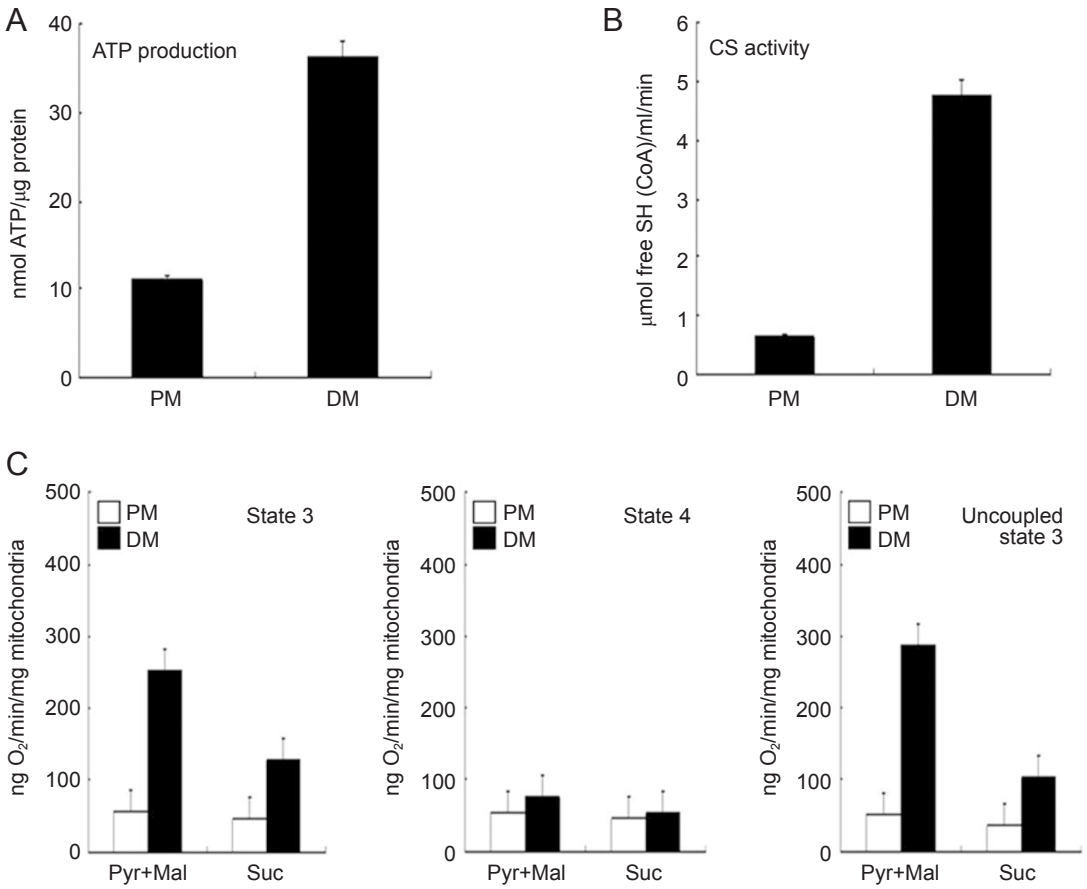

Figure 6 Enhancement of mitochondrial functions during muscle differentiation. Cells were induced to differentiate for 5 days in DM. **(A)** Intracellular ATP content. **(B)** Citrate synthase activity. **(C)** Respiratory activities of the mitochondria. The substrate concentrations were as follows: 2.5 mM pyruvate (Pyr), 2 mM malate (Mal), and 5 mM succinate (Suc).

Elimination of mitochondrial ROS impairs muscle differentiation

Mitoquinone (MitoQ) and MitoTEMPOL are mitochondria-targeted antioxidants derived from ubiquinone and TEMPOL (4-hydroxy-2,2,6,6 tetramethylpiperidine-1-oxy radical), respectively [25, 26]. Therefore, to investigate whether mROS stimulated muscle differentiation, we depleted mROS using MitoQ and MitoTEMPOL and observed their effects on muscle differentiation. These antioxidants suppressed morphological changes, MHC expression in myotube formation (Figure 3A), and the activity of the MCK promoter (Figure 3B). The amount of mH_2O_2 measured using Amplex Red was significantly decreased (Figure 3C). Consistent with a decrease in mROS, the expression level of MnSOD in mitochondrial fractions was also decreased (Figure 3D).

Recently, mitochondria-targeted adenoviral recombinant catalase (rAd.CMVMCAT, MCAT) was shown to catalyze the conversion of mH_2O_2 into H_2O within mitochondria [27]. To further determine the role of mH_2O_2 in muscle differentiation, we transduced MCAT into the mitochondria and then observed the muscle differentiation processes. Adenoviral recombinant catalase (rAd.CMVCAT, CAT) was also transduced into cells. The transduction efficiency was evaluated using a β-gal assay (data not shown) and western blotting (Figure 4A). Both proteins were significantly expressed in their targeted sites. The cells transduced with MCAT did not differentiate (Figures 4B). Consistently, the amount of mH_2O_2 and the induction of MnSOD were dramatically decreased compared with mock cells (Figures 4C and D). The CAT-transduced cells did not differentiate either, but their mH_2O_2 and MnSOD levels did not decrease to the same extent as they did in MCAT-transduced cells. Considering that cytosolic CAT also catalyzes the conversion of H_2O_2 diffused from the mitochondria into the cytosol to H_2O and, thus, lessens oxidative stress in mitochondria, our results are not unexpected.

Mitochondrial alterations during muscle differentiation

Because increased mH_2O_2 is an important signal for muscle differentiation, we investigated whether mitochondrial changes occurred during muscle differentiation. Mitochondrial transcription factor A (TFAM) is encoded by nuclear DNA and regulates mitochondrial biogenesis and mitochondrial DNA (mtDNA) transcription [1, 28]. The mitochondrial genome encodes some mETC complex subunits, such as ND1-6 and ND4L of complex I, Cyt *b* of complex III, COX I-III of complex IV, and ATPase 6 and 8 of complex V, along with mitochondrial rRNA and tRNA [29]. We first investigated whether TFAM was induced and found that it was increasingly induced during muscle differentiation (Figure 5A). In addition, the levels of ND4 mRNA and 16S rRNA encoded by mtDNA were up-regulated during muscle differentiation (Figure 5B). As shown in Figure 5C, transmission electron microscopy (TEM) images showed an increase in the numbers and sizes of the mitochondria and the development of cristae in DM-stage cells compared with PM-stage cells. Because of the mitochondrial changes induced by TFAM, we further examined the effect of TFAM on muscle differentiation. We suppressed the expression of TFAM using a specific small interfering RNA (siRNA). The TFAM-siRNA completely suppressed TFAM expression (Figure 5D) and blocked muscle differentiation (Figures 5E). These data reveal that TFAM is critical for muscle differentiation.

Next, we examined whether alterations in mitochondrial functions, such as ATP synthesis, metabolism and

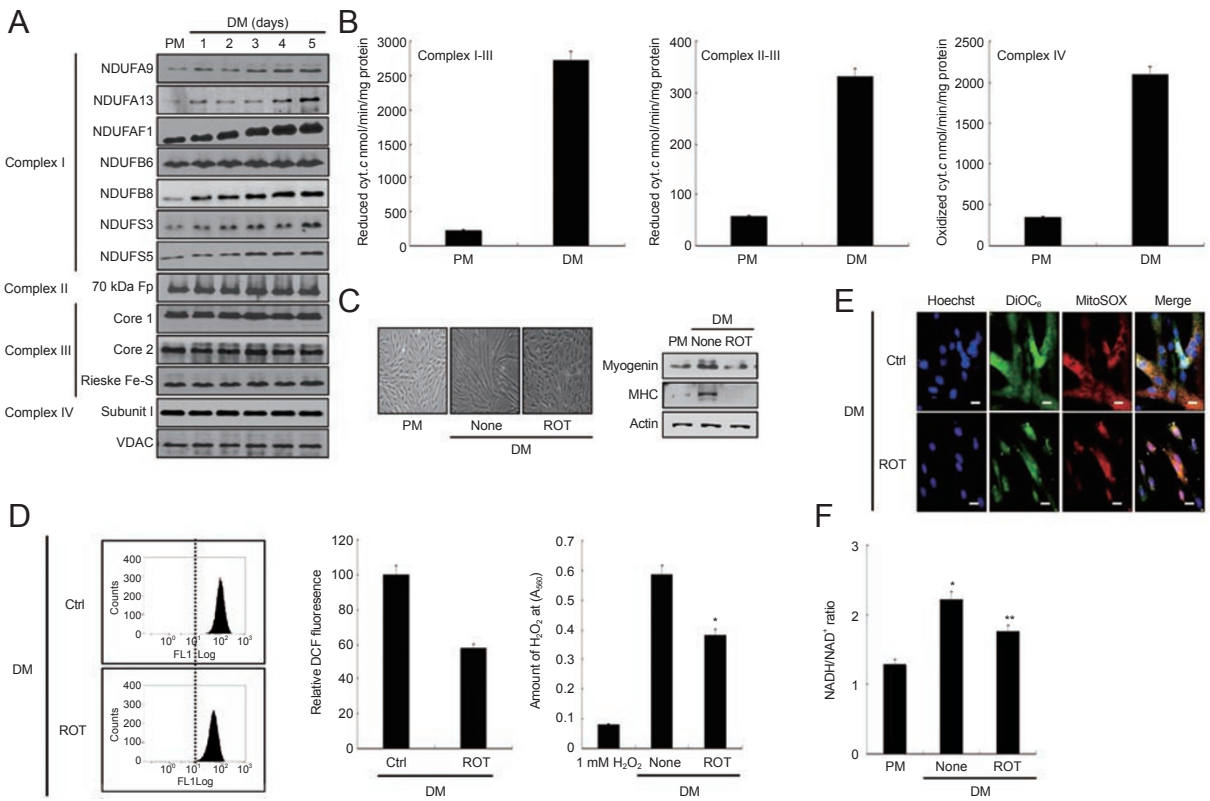

Figure 7 H_2O_2 dismutated from mETC complex I-derived $O_2^{\cdot -}$ is crucial for muscle differentiation. **(A)** Expression patterns of various subunits of mETC complexes during muscle differentiation. **(B)** Activities of complex I-III (left), II-III (middle), and IV (right). To observe how rotenone affects muscle differentiation, mROS generation, and mitochondrial NADH/NAD^+ ratio, rotenone (ROT, 10 nM) was added to cells in DM. **(C)** Differentiation was evaluated through morphological changes and western blot analysis using antibodies against myogenin and MHC. **(D)** ROS levels were measured using flow cytometry after loading with DCF-DA, and relative DCF fluorescence is shown compared with DM control (Ctrl) (left and middle). H_2O_2 levels in isolated mitochondria (right). A total of 1 mM H_2O_2 was used as a standard control. Data represent means ± SE, $n = 3$. *$P < 0.001$ vs absence of drug (None) in DM. **(E)** Verification of the effect of complex I inhibition on mitochondrial ROS levels via confocal microscopy. Mitochondria tracker $DiOC_6$, green; mitochondrial ROS indicator MitoSOX, red; nuclear indicator Hoechst 33342, blue. Scale bar, 20 μm. **(F)** Change in the mitochondrial NADH/NAD^+ ratio. The NADH and NAD^+ concentrations were measured as described in Materials and Methods. Data represent means ± SE, $n = 3$. *$P < 0.001$ vs PM. **$P < 0.001$ vs absence of drugs (None) in DM.

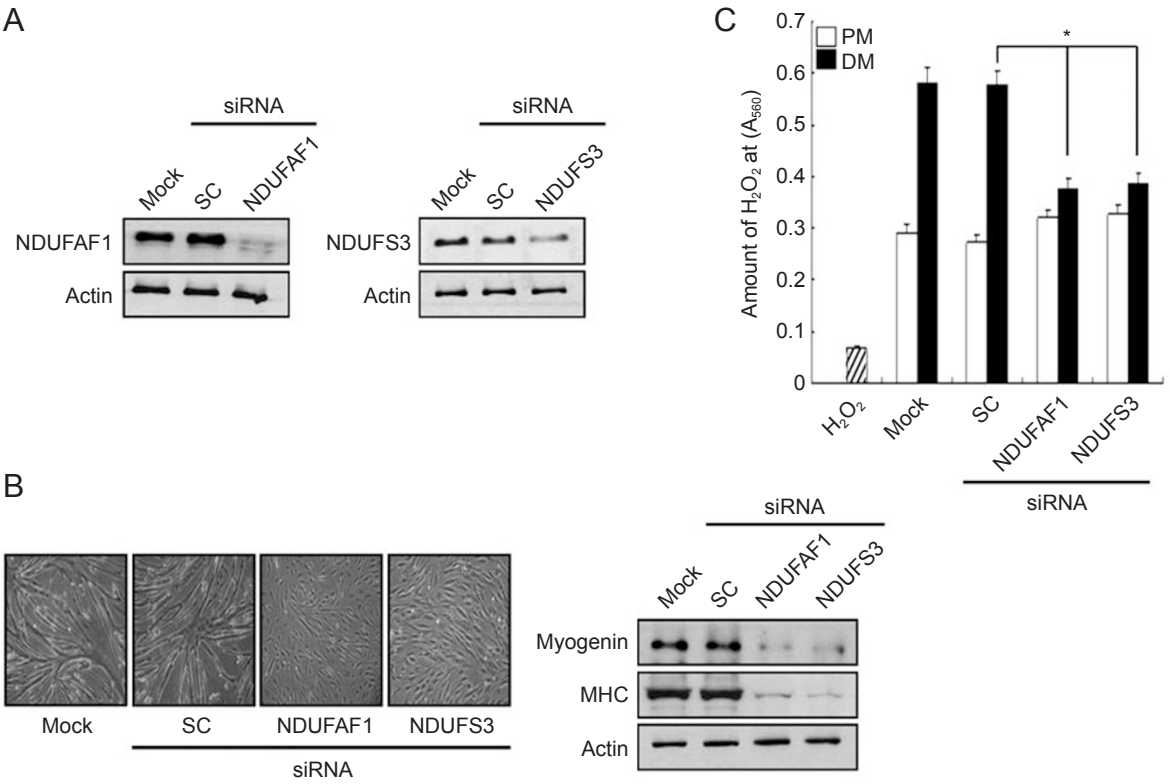

Figure 8 Knockdown of mETC complex I subunits NDUFAF1 and NDUFS3 prevents muscle differentiation. Cells were transfected with siRNAs specific to NDUFAF1 and NDUFS3 and then exposed to PM or DM for 5 days, respectively. **(A)** Knockdown of NDUFAF1 and NDUFS3 using specific siRNAs. **(B)** Morphological changes and expression patterns of myogenin and MHC. Actin was used as a loading control. **(C)** H_2O_2 levels in isolated mitochondria. Scrambled control siRNA (SC) was used as a control for all of the knockdown studies. A total of 1 mM H_2O_2 was used as a standard control. Data represent means ± SE, n = 3. *P < 0.001 vs SC transfected cells in DM.

respiration, occurred during muscle differentiation. We first measured ATP levels and the activity of citrate synthase, a matrix marker enzyme. The results showed an approximately four-fold increase in intracellular ATP levels (Figure 6A) and a five-fold increase in citrate synthase activity (Figure 6B) in DM-stage cells compared with PM-stage cells. The measured respiration rate showed that state 3 respiration in DM-stage cells was increased approximately five-fold using the NADH-dependent substrates pyruvate and malate compared with PM-stage cells. The state 3 respiration in DM-stage cells was increased approximately two-fold using the $FADH_2$-dependent substrate succinate compared with PM-stage cells (Figure 6C, left). The increased respiration rate was inhibited by the ATP synthase inhibitor oligomycin (state 4 respiration) (Figure 6C, middle). Furthermore, state 3 respiration was slightly stimulated by the uncoupler CCCP (Figure 6C, right). These results indicate that mitochondrial changes and functional activation by the induced TFAM occur during muscle differentiation.

H_2O_2 dismutated from complex I-derived $O_2^{\cdot-}$ is crucial for muscle differentiation

Because ATP levels, citrate synthase activity and respiration were increased during muscle differentiation, we further investigated whether mETC complexes changed during muscle differentiation. First, we performed western blotting using antibodies against various subunits of mETC complexes to investigate the change in expression level of each mETC complex subunit. As shown in Figure 7A, three subunits of complex I (NDUFA9, NDUFAF1 and NDUFB8) were strongly up-regulated and the other four (NDUFA13, NDUFB6, NDUFS3 and NDUFS5) were increased slightly after exposure to DM conditions. Interestingly, other complex subunits did not show any changes. Next, we measured the activities of complex I-III, II-III and IV as described in Materials and methods. All mETC complex activities were increased during differentiation: complex I-III activity increased approximately twelve-fold, while complex II-III and IV activities increased six-fold (Figure 7B). These results

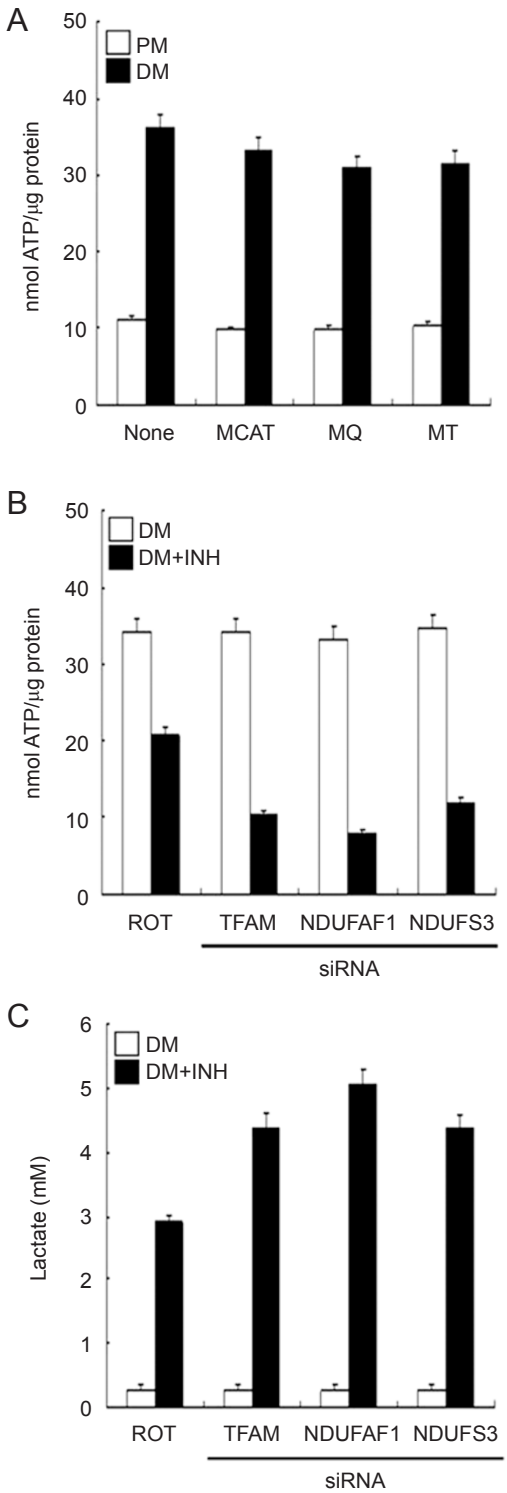

Figure 9 Determination of metabolic state. **(A)** ATP contents. Cells were exposed to PM and DM for 5 days with or without mitochondria-targeted catalase (MCAT, 100 to 200 viral particles/cell) or 200 nM MitoQ (MQ) and 100 μM MitoTEMPOL (MT). **(B, C)** Complex I-inhibited cells (DM + INH) were exposed to DM for 5 days to measure ATP content **(B)** and lactate production **(C)**. INH: rotenone (ROT) and siRNAs (TFAM, NDUFAF1, NDUFS3).

indicate that mETC complex I is more activated than the other complexes during muscle differentiation.

Although many studies have reported that complex I and III are major sites of $O_2\cdot^-$ generation in mitochondria [4-6], we hypothesized that the increased mROS generation during muscle differentiation occurred at complex I through reverse electron transport (RET) because of the increased expression levels of only mETC complex I subunits and a greater increase in complex I-III activity than the others during muscle differentiation. RET was first observed in single mitochondrial particles respiring on succinate. Extensive $O_2\cdot^-$ generation by RET occurs under conditions of high proton-motive force with electron supply to the CoQ pool. Then, electrons are reverse transported from $CoQH_2$ to complex I to reduce NAD^+ to NADH at the FMN site. Rotenone blocks electron back-flow into complex I through the CoQ-binding site and thus abolishes $O_2\cdot^-$ generation at complex I during RET [5]. To determine whether RET occurred within cells during the physiological muscle differentiation

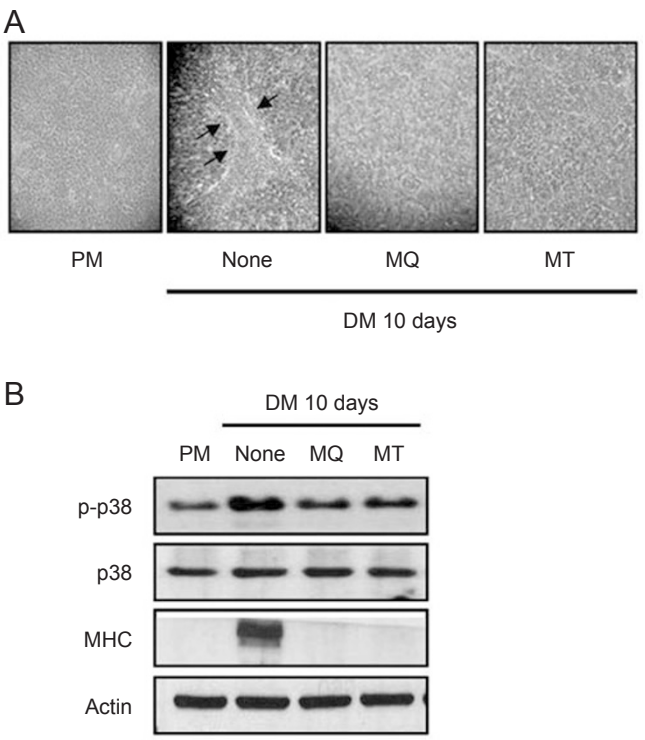

Figure 10 Role of mROS in P19CL6 cell differentiation. P19CL6 cells were exposed to DM for 10 days with or without 200 nM MitoQ (MQ) or 100 μM MitoTEMPOL (MT). **(A)** Morphological changes. Arrows indicate differentiated cells. **(B)** Effect of MitoQ and MitoTEMPOL on MHC expression and p38MAPK activation in P19CL6 cells. Actin was used as a loading control.

process, we performed several experiments with indirect parameters because there are no experiments devised to directly assess RET within cells. We observed the effect of rotenone, a complex I inhibitor, on muscle differentiation, mROS generation, and the mitochondrial NADH/NAD^+ ratio. The results showed that cells did not differentiate during rotenone exposure (Figure 7C). The high level of ROS in DM, as revealed using FACS analysis after 2′-7′-dichlorodihydrofluorescein diacetate (DCF-DA) staining, was remarkably decreased in response to rotenone treatment (Figure 7D, right and middle). In addition, in mitochondria isolated from cells that were treated with rotenone during muscle differentiation, the amount of mH_2O_2 was also decreased (Figure 7D, left). As shown in Figure 7E, when complex I was inhibited by rotenone, $O_2\cdot^-$ was decreased in the mitochondria compared with control DM conditions. Next, we observed changes in the mitochondrial NADH/NAD^+ ratio during muscle differentiation and assessed the effect of rotenone on the mitochondrial NADH/NAD^+ ratio. The mitochondrial NADH/NAD^+ ratio was increased two-fold during muscle differentiation. Rotenone decreased the increased mitochondrial NADH/NAD^+ ratio (Figure 7F). From these results, we conclude that mROS are generated at complex I through RET within intact cells during muscle differentiation.

Next, we further tested the involvement of mETC complex I in muscle differentiation by knocking down the complex I subunits using siRNA. Among the 45 different subunits of complex I [30], NDUFAF1, an assembly chaperone [31], and NUDFS3, a hydrogenase module [32], were chosen for this experiment. The respective siRNAs completely suppressed their target protein expression levels after 48 h of cultivation in PM (Figure 8A). In addition, they completely blocked muscle differentiation processes, as shown in Figure 8B. The amount of mH_2O_2 measured in mitochondria isolated from the cells transfected with NDUFAF1 and NDUFS3 siRNAs was also decreased compared with mock and scrambled control-siRNA transfected cells (Figure 8C). These results suggest that among the mETC complexes, complex I is a major ROS generation site and provides a pivotal signal for muscle differentiation.

Evaluation of cellular energy status

Because ATP can also be depleted after inhibition of complex I and ATP depletion can block differentiation, we next tested whether scavenging of mROS or the inhibition of complex I activity affected intracellular ATP levels. In cells treated with MCAT, MitoQ and MitoTEMPOL, intracellular ATP levels were not changed (Figure 9A). However, as shown in Figure 9B, intracellular ATP levels in all cells with complex I activity inhibited by rotenone and siRNAs and in TFAM-suppressed cells using siRNA were significantly decreased compared with control DM stage cells (Figure 9B). The decrease in ATP levels in those cells was accompanied by large increases in lactate production (Figure 9C), indicating that complex I activity-inhibited cells and cells in which TFAM was suppressed using siRNA alternate their metabolic state with the glycolytic pathway for energy recovery.

Role of mH_2O_2 in P19CL6 cell differentiation

To further study the role of mH_2O_2 in muscle differentiation, we tested whether mH_2O_2 was involved in the differentiation of P19CL6 cells, a clonal derivative of mouse P19 EC cells. For these experiments, we treated cells with MitoQ and MitoTEMPOL to deplete mROS and observed changes in cell morphology, MHC expression level, and p38 MAPK activation. p38 MAPK is one of the key myogenic signaling molecules. The results showed that MitoQ and MitoTEMPOL inhibited differentiation of and p38 MAPK activation in P19CL6 cells (Figure 10), indicating that mH_2O_2 also has a stimulatory effect on the differentiation of P19CL6 EC cells.

Discussion

Here, we show for the first time that mH_2O_2 that is dismutated from $O_2\cdot^-$, which is produced at mETC complex I by RET, by induced MnSOD acts as a signaling molecule for muscle differentiation. The stimulatory effect of mH_2O_2 on muscle differentiation was confirmed because the elimination of mROS by mitochondria-targeted antioxidants MitoQ and MitoTEMPOL, mitochondria-targeted recombinant catalase, and the inhibition of complex I by rotenone and siRNAs decreased mROS generation and impaired muscle differentiation.

$O_2\cdot^-$ is mainly generated in complex I and III in mitochondria. In the case of muscle differentiation, we think that complex I is the major site for $O_2\cdot^-$ generation, although complex III cannot be ruled out for $O_2\cdot^-$ generation, for the following reasons. First, only complex I subunits were up-regulated, while other complex subunits were not changed. Second, the activation rate of complex I-III was much higher than that of complex II-III and IV. Third, the inhibition of complex I by rotenone significantly decreased the level of mROS and the mitochondrial NADH/NAD^+ ratio in DM and also suppressed muscle differentiation. The effects of rotenone on ROS generation at complex I are complicated and difficult to interpret due to the multiple effects of rotenone depending on the cell type, substrate, activity of the matrix antioxidant system and extracellular stress [5, 11]. In fact,

there are two modes of $O_2\cdot^-$ production from complex I. In the first mode, a high NADH/NAD^+ ratio in the mitochondrial matrix leads to $O_2\cdot^-$ production at the FMN site of complex I when the respiratory chain is inhibited by damage, mutation, ischemia or loss of cytochrome *c*. In this case, rotenone increases $O_2\cdot^-$ production by electrons that have accumulated on NADH, reducing FMN. In the second mode, complex I produces large amounts of $O_2\cdot^-$ during RET. When cells highly reduce the coenzyme Q (CoQ) pool with a concomitant significant increase in proton-motive force, electrons are reverse transported from $CoQH_2$ into complex I to reduce NAD^+ to NADH at the FMN site. In this case, rotenone blocks electrons from entering complex I from $CoQH_2$ and thereby decreases ROS production [5]. In general, RET is observed in isolated mitochondria respiring on succinate. However, it has been reported that RET and RET-associated ROS production occur through high activity of the TCA cycle and mitochondrial respiration in the presence of NADH-dependent substrates, such as pyruvate and malate, in brain mitochondria and brain synaptosomes [33, 34]. We observed increases in ATP levels, citrate activity, mitochondrial respiration, and mETC complex activities during muscle differentiation, indicating that metabolism is enhanced during muscle differentiation. Therefore, we hypothesize that the increased NADH and $FADH_2$ levels due to induced metabolism provide complex I and II, respectively, with more electrons and that the excessive electron influx into CoQ through complexes I and II induces RET and RET-associated ROS generation. Although RET occurs by electron inflow through complex II in isolated mitochondria respiring on succinate, we propose that electrons entering complex I are also involved in RET because electron flow into CoQ within intact cells occurs not only from $FADH_2$ through complex II but also from NADH through complex I. We observed that the knock-down of complex I using siRNAs specific to NDUFAF1 and NDUFS3, which are involved in the assembly and hydrogenase activity of complex I, respectively, reduced mROS production (Figure 8), indicating that complex I is the entry point for electrons from NADH into the mETC during muscle differentiation. Based on these results, we conclude that $O_2\cdot^-$, which is dismutated to H_2O_2 by increased MnSOD, is mainly generated at complex I through RET by enhanced metabolism during muscle differentiation.

The stoichiometry of complex I is 2 ($4H^+/2e^-$) in most cases. However, Freeman and Lemasters concluded that the H^+/e^- stoichiometry of complex I was 2.5 during RET in mitochondria [35]. RET-associated $O_2\cdot^-$ production depends on the ΔpH (pH gradient) component of the Δp (proton-motive force). Because we found enhanced $O_2\cdot^-$ production by RET during muscle differentiation, we think that the stoichiometry of complex I may be increased up to 2.5 during muscle differentiation, even though we did not perform any experiments to evaluate the H^+/e^- stoichiometry of complex I.

Concluding that the $O_2\cdot^-$ generated at complex I stimulated muscle differentiation is complicated by the fact that inhibition of complex I by rotenone and siRNAs specific to complex I subunits decreased both ATP and mROS levels. Compared with the proliferative stage, ATP levels, citrate synthase activity, and state 3 respiration were significantly increased during differentiation, indicating that mitochondria in DM-stage cells have a high capacity to synthesize ATP (Figure 6). These observations strongly suggest that ATP depletion might impair muscle differentiation. Therefore, we measured ATP levels after MCAT, MitoQ, and MitoTEMPOL treatments and found that these mROS scavengers did not affect ATP levels. However, they impaired muscle differentiation and decreased mROS levels, contrary to rotenone and siRNAs against complex I subunits, both of which not only blocked muscle differentiation but also depleted ATP. Furthermore, decreased ATP synthesis in mitochondria in response to rotenone and siRNAs against complex I subunits seemed to be compensated by increased glycolysis (Figure 9). From these results, we conclude that mETC complex I contributes to muscle differentiation by generating higher amounts of $O_2\cdot^-$ that is, in turn, dismutated to H_2O_2, which then acts as a pivotal signaling molecule for muscle differentiation.

TFAM is encoded by nuclear DNA and regulates mitochondrial biogenesis and mtDNA transcription [1, 28]. In this study, mitochondrial alterations in response to induced TFAM, such as mtDNA activation and mitochondrial biogenesis, were found to be critical for muscle differentiation (Figure 5). Moreover, increases in ATP levels, citrate synthase activity, and mitochondrial respiration were observed during muscle differentiation (Figure 6). Consistent with our observations, it has been reported that TFAM expression is linked to cellular energy needs [36]. Therefore, we hypothesize that mROS are increased due to mitochondrial alterations and functional activations by TFAM induction during muscle differentiation. Interestingly, only complex I subunits were up-regulated during muscle differentiation (Figure 7A). The discrepancy in expression levels of mETC complex subunits has been reported previously [37, 38] and is consistent with our results.

mROS have been reported to function mainly as oxidative stress molecules rather than signaling molecules and have thus been implicated in many pathological conditions and aging processes accompanied with cell

damage, such as necrotic or apoptotic cell death [4]. Therefore, our argument that mH_2O_2 stimulates muscle differentiation seems unusual. However, several observations supporting our concept have recently been reported. For example, it has been reported that mROS perform physiological functions, such as the prevention of TNF-induced apoptosis, by enhancing the NF-κB-mediated expression of antiapoptotic proteins [12], the regulation of vascular endothelial cell function, including recovery of relaxation responses and maintenance of Ca^{2+} homeostasis after mechanical stimuli [39], the induction of nutrient sensing within the hypothalamus [11], and maturation and antigen capture in monocytes and monocyte-derived dendritic cells [40].

Mitochondria and Nox have been considered intracellular ROS sources. Previously, we reported that ROS generated from Nox2 are involved in muscle differentiation. However, we observed that ROS levels were not completely decreased despite Nox2 knockdown, which also exhibited an incomplete suppression of muscle differentiation [20]. In addition, when the Nox1 subunit was specifically suppressed using siRNA, muscle differentiation was only slightly inhibited (data not shown). Consequently, we think that mitochondria are an additional source, along with Nox, for ROS generation to achieve complete muscle differentiation.

In summary, we have shown that $O_2{\cdot}^-$ production at mETC complex I through RET is increased and $O_2{\cdot}^-$ is dismutated to H_2O_2 by induced MnSOD, which in turn stimulates muscle differentiation. The stimulatory effect of mH_2O_2 on muscle differentiation was observed in both H9c2 and P19CL6 EC cells, suggesting that diverse cells, including cardiac stem cells, require ROS generation at mETC complexes to fully differentiate. It will be valuable to further explore the physiological roles of mETC complexes in many cellular processes, including the differentiation of diverse cells, at the molecular level in the future.

Materials and Methods

Chemicals and reagents

Dulbecco's modified Eagle's medium/F-12 (DMEM/F-12), α-MEM, donor calf serum, fetal bovine serum, and horse serum were purchased from Gibco-BRL (Grand Island, NY, USA). Antibodies against each subunit of the mitochondrial complexes were purchased from MitoScience (Eugene, OR, USA). Antibody against NDUFS5 was provided by GeneTex (Irvine, CA, USA). Antibodies against NDUFAF1 and TFAM were provided by Santa Cruz Biotechnology (Santa Cruz, CA, USA). MitoQ was acquired from Dr Michael P Murphy. MitoTEMPOL was provided by Alexis Biochemicals (San Diego, CA, USA). Rotenone, 2-thenoyltrifluoroacetone (TTFA), antimycin A, and actinomycin D were acquired from Sigma Aldrich (St Louis, MO, USA). Stigmatellin was provided by Fluka (St Louis, MO, USA).

Cell culture

H9c2 rat cardiac myoblasts were grown in DMEM/F-12 containing 10% (v/v) donor calf serum (proliferation medium, PM). Cells were induced to differentiate by placing them in DMEM/F-12 containing 1% (v/v) horse serum. Full differentiation was achieved 5-6 days after the induction of differentiation. P19CL6 cells (RIKEN BRC, Ibraki, Japan), clonal derivatives of mouse P19 EC cells, were grown in α-MEM containing 10% fetal bovine serum. The cells were induced to differentiate with a standard medium containing 1% DMSO [41].

Location of mitochondrial ROS using confocal microscopy

After being induced to differentiate, the live cells were incubated with 5 μM MitoSOX and 50 nM $DiOC_6$ (Molecular Probes, Invitrogen, Carlsbad, CA, USA). After being washed, cells were fixed in 4% formaldehyde. Then, 10 μM Hoechst 33342 (Sigma Aldrich) was loaded. The cells were then washed with PBS. The stained cells were monitored using an LSM510 confocal laser microscope (Carl Zeiss, Thornwood, NY, USA).

Preparation of mitochondrial fractions and mitochondrial proteins

Preparations of mitochondrial fractions and mitochondrial proteins were performed as described previously [42]. Cells were suspended in lysis buffer (250 mM sucrose, 0.1 mM EDTA, and 2 mM HEPES, pH 7.4) and homogenized, and mitochondria were isolated using differential centrifugation. The isolated mitochondria were subjected to mitochondrial H_2O_2 measurement. For western blotting, mitochondria were lysed in lysis buffer (Intron Biotechnology, Kyunggi, Korea).

Mitochondrial H_2O_2 measurement

The levels of mitochondrial H_2O_2 were determined using a modified method that monitors the absorbance of resorufin, a reaction product of Amplex Red [43, 44]. A total of 100 μl of reaction buffer (120 mM KCl, 3 mM HEPES free acid, 1 mM EGTA, and 0.3% BSA, pH 7.2, at 37 °C), including 50 μM Amplex Red (Molecular Probe, Invitrogen), 6 U/ml HRP, and 30 U/ml SOD, was added to each microplate well and then pre-warmed at 37 °C for 10 min. Then, the reaction was started by adding 35 μg of mitochondrial fractions re-suspended in 100 μl of reaction buffer. After 30 min, the absorbance of the reaction mixtures was measured at 560 nm using a fluorescence microplate reader (Bio-Rad, Richmond, CA, USA).

Detection of intracellular H_2O_2 using flow cytometry

Intracellular H_2O_2 was measured as previously described [16]. Briefly, H_2O_2 was measured using DCF-DA. The cells were loaded with 10 μM DCF-DA, and fluorescence was measured using a flow cytometer (FACSCalibur, Becton-Dickinson, Franklin Lakes, NJ, USA). The mean DCF fluorescence intensity was measured with excitation at 488 nm and emission at 525 nm.

RNA extraction and semiquantitative RT-PCR

For the analysis of MnSOD mRNA, total RNA was prepared from cells using TRIzol Reagent (Invitrogen). Total RNA (1 μg) was amplified using a two-step protocol using AMV reverse-

transcriptase (Promega, Madison, WI, USA) and Taq polymerase. Primers for amplifying MnSOD transcripts were as follows: forward, 5′-TGACCTGCCTTACGACTATG-3′; reverse, 5′-GCTGCAATGCTCTACACTAC-3′. The PCR was conducted for 5 min at 95 °C followed by 25 cycles of 95 °C for 1 min, 55 °C for 1 min, and 72 °C for 1 min.

Real-time quantitative RT-PCR

The mRNA levels of MnSOD, mtDNA-encoded protein ND4, mitochondrial 16S rRNA, and GAPDH were measured using a SYBR Green-based real-time RT-PCR using SYBR® Green PCR Master Mix (Applied Biosystems, Foster City, CA, USA). The primer sequences designed by Primer 3 and UCSC In-Silico PCR were as follows: MnSOD forward, 5′-CACTGTGGCTGAGCTGTTGT-3’; MnSOD reverse, 5′-TCCAAGCAATTCAAGCCTCT-3′; ND4 forward, 5′-CACCTCCTACAGCTTTCTAGT-3′; ND4 reverse 5′-TGCGGAGAATGTTATGATGAG-3′; 16S rRNA forward, 5′-AAGCGTTCAAGCTCAAGCTCAACATAC-3′; 16S rRNA reverse, 5′-AATCTTTCCTTAAAGCACGCC-3′; GAPDH forward, 5′-CATGTTTGTGATGGGTGTGA-3′; GAPDH reverse, 5′-TCCACAGTCTTCTGAGTGGC-3′. Real-time PCR amplification was conducted using TaqMan Universal Mastermix (PE Applied Biosystems, Branchburg, NJ, USA). The thermal cycler conditions were as follows: 10 min at 95 °C followed by 50 cycles of 95 °C for 15 s and 60 °C for 1 min. Finally, the samples were held at 65 °C for 5 min, and melting curve analyses were performed from 65 to 95.1 °C. Calculations were based on the "Delta-Delta method" using the equation R (ratio) = $2^{-[\Delta CT^{sample}-\Delta CT^{control}]}$ [45]. The integrity of amplified DNA was confirmed using the determination of the melting temperature. The data were expressed as fold change of the treatment groups in relation to the control (GAPDH).

Preparation of nuclear extracts

Nuclear extracts were prepared as described previously [16].

Construction of the plasmid for MnSOD promoter analysis

The MnSOD promoter sequence was analyzed using MalInspector by Genomatrix (http://www.genomatix.de). For construction of the luciferase reporter plasmid, 1 023 bp of the MnSOD promoter sequence containing three NF-κB binding sites were amplified using PCR. The deleted fragments were cloned into the pGL3 basic vector with KpnI and XhoI (Promega). For mutational analysis, the NF-κB binding site, which exists within the −960 region of the MnSOD promoter, was mutated using PCR-based site-directed mutagenesis. Primers used for constructing luciferase reporters containing various regions of the MnSOD promoter or mutated NF-κB binding sites are as follows: pGL3-SOD2/450 forward, 5′-AAGGTACCGGCTCTGACCAGCAGCAGGGCCC-3′; pGL3-SOD2/600 forward, 5′-CCCGGTACCCACACTAAAAC-CTGAGATG-3′; pGL3-SOD2/900 forward, 5′-CCCGGTAC-CCCGTAAGT-CAACAAAGGG-3′; pGL3-SOD2/1023 forward, 5′-AAGGTACCAATTCCCCTTACCAAGCCCAGT-3′; pGL3-SOD2 /1023 reverse, 5′-AACTCGAGACAACATTGCTGAG-GCGCCCAC-3′; pGL3-SOD2/960M forward, 5′-CAAAGGGGGT-G**A**GAAAAA**T**CACCCGGAACTAC-3′; pGL3-SOD2/960M reverse, 5′-GTAGTTCCGGGTG**A**TTTTTC**T**CACCCCCTTTG-3′.

Luciferase assay

Cells were transfected with 0.5 μg of the pGL3 basic-derived plasmids along with the internal control plasmid pSV-β-gal (Promega). Cells were incubated in PM or DM and harvested in lysis buffer. Luciferase and β-gal activities were measured using a microplate reader (Bio-Rad) using 20 μl of each cell lysate. The luciferase activity was normalized on the basis of β-gal activity.

Electrophoretic mobility shift assay

EMSA was performed as described previously [15] using the following oligonucleotides derived from the MnSOD promoter sequence: NF-κB-WT, 5′-AGGGGGTGG-GAAAAACCACCCGGA-3′; NF-κB-Mutant, 5′-AGGGGG-TG**A**GAAAAA**T**CACCCGGA-3′. Sense and antisense strands of oligonucleotides were annealed and labeled with [γ-^{32}P]ATP (Amersham Biosciences, Little Chalfont, UK). For the competition study, a 100-fold molar excess of unlabeled oligonucleotides was added to the reaction mixture prior to the addition of the radiolabeled probe.

Chromatin immunoprecipitation

Conventional ChIP was conducted as described previously [46], except that cross-linked H9c2 chromatin was subjected to immunoprecipitation with an antibody against the p65 subunit of NF-κB. The MnSOD promoter containing a binding site of NF-κB was amplified using the following primers: forward, 5′-CCCTCCTGGTAACAGTGTTAG-3′ and reverse, 5′-GCCTACTAAGGATGACTGGG-3′.

Recombinant adenovirus-mediated expression of MCAT

Recombinant adenovirus was used for the transient induction of MCAT expression. Adenoviral constructs were purchased from the University of Iowa Vector Core Laboratory and contained either human CAT cDNA (rAd.CMVCAT, CAT) or a chimeric cDNA composed of the human MnSOD mitochondrial localization signal and human CAT cDNA (rAd.CMVMCAT, MCAT). H9c2 cells were transduced with the various recombinant adenovirus particles at a multiplicity of infection ranging from 100 to 200 viral particles/cell in DM [27]. To determine the transduction efficiency, we co-transduced a recombinant adenovirus harboring the bacterial enzyme β-galactosidase (rAd.lacZ) and measured β-gal activity.

RNA interference

The siRNA mixture specific to TFAM, NDUFAF1, and NDUFS3 and the scrambled control siRNA were prepared by Dharmacon, Inc. (Chicago, IL, USA). The following sequences were used: TFAM siRNA mixture, oligo 1, 5′-GAUGAUA-GAUUCGUUAUG -3′; oligo 2, 5′-CUACCCAAAUUUAAAGCUA -3′; oligo 3, 5′-GAAGCUGUGAGCAAGUAUA -3′; and oligo 4, 5′-GAGUUCAUACCUUCGAUUU -3′; NDUFAF1 siRNA mixture, oligo 1, 5′-GCGAUGAUCUCCAGGAUUC-3′; oligo 2, 5′-GAUGUA-CAGUUACUUCAUG-3′; oligo 3, 5′-GAUAAGACAAUUGGAG-GUA-3′; and oligo 4, 5′-CUUGGAUGGUGAAUAUUAA-3′; and NDUFS3 siRNA mixture, oligo 1, 5′- UGGCUGAAAUCUUAC-CUAA-3′; oligo 2, 5′ -GGAUUCGUGUGAAGACCUA-3′; oligo 3, 5′-UCUCAAGGAUCAUACCAAU-3′; and oligo 4, 5′-CGAGU-GAUGUAACCCACAA-3′. siRNAs (0.5 μg/ml) were transfected into cells using Lipofectamine 2000 (Invitrogen). The efficiency of siRNA interference of TFAM, NDUFAF1, and NDUFS3 was monitored via western blot.

Transmission electron microscopy

Cells were fixed in Karnovsky's fixative solution (1% paraformaldehyde, 2% glutaraldehyde, 2 mM calcium chloride, and 100 mM cacodylate buffer, pH 7.4) for 2 h, washed with cacodylate buffer, and postfixed in 1% osmium tetroxide and 1.5% potassium ferrocyanide for 1 h. Cells were dehydrated through a graded ethanol series and embedded in propylene oxide and EPON:propylene oxide (1:1). Cells were sectioned using Reichert Ultracut (Leica, Cambridge, UK). After being stained with uranyl acetate and lead citrate, cells were observed and photographed under a transmission electron microscope (Zeiss EM 902 A, Leo, Oberkohen, Germany).

Measurement of oxygen consumption rate

The oxygen consumption rate was measured polarographically using a Clark-type electrode (YSI Inc., Yellow springs, OH, USA) in an all-glass reaction chamber with magnetic stirring at 37 °C. Mitochondria (0.3 mg/ml) were suspended in reaction medium containing 125 mM KCl, 10 mM MOPS, pH 7.2, 2 mM $MgCl_2$, 2 mM KH_2PO_4, 10 mM NaCl, 1 mM EGTA, and 0.7 mM $CaCl_2$. State 3 respiration was initiated by the addition of 150 μM ADP. A total of 1 μg/ml oligomycin was used to induce state 4 respiration. A total of 0.5 μM CCCP was used to stimulate uncoupled state 3 respiration.

Measurement of citrate synthase activity

Citrate synthase activity was measured using a citrate synthase assay kit (Sigma) as described by the manufacturer. Citrate synthase activity was measured spectrophotometrically at 412 nm using 2 μg of isolated mitochondria.

Measurement of intracellular ATP content and lactate production

ATP concentration was determined using the ATP bioluminescent assay kit supplied by Sigma. ATP contents were calculated as nmol ATP per microgram of protein.

To measure lactate production, cells were incubated for 10 min in a buffer without glucose containing 110 mM NaCl, 5 mM KCl, 1 mM $MgCl_2$, 4 mM Na_2PO_4, and 50 mM Na-HEPES, pH 7.4. The cells were then washed twice in the same buffer, and glycolysis was initiated by the addition of 20 mM glucose. Next, 100 μl of cell suspension was withdrawn from the culture plates and centrifuged. The supernatants were added to 900 μl of a medium containing 467 mM glycine, 280 mM hydrazine sulfate, 2.6 mM EDTA, pH 9.5, and 1 mM NAD^+. The reaction was started by adding 10 IU of LDH. The concentration of lactate released into the buffer was measured using an enzyme-linked assay system [47].

Measurement of mETC complex activity

NADH-cytochrome *c* oxidoreductase activity (complex I-III), succinate cytochrome *c* reductase activity (complex II-III), and cytochrome *c* oxidase (complex IV) activity were measured as previously described [48]. The reaction mixture for the complex I-III activity assay consisted of 100 mM potassium phosphate buffer, pH 7.4, 5 mM KCN, 1 mM β-NADH, and 50 μg of cell lysate. The reaction was initiated by the addition of 100 μM cytochrome *c*, and the increase in absorbance was monitored 1 min before and 1 min after the addition of 100 nM rotenone. Complex I-III activity was considered the rotenone-sensitive rate of NADH-induced cytochrome *c* reduction at 550 nm. The reaction mixture for the complex II-III activity assay consisted of 100 mM potassium phosphate buffer, pH 7.4, 5 mM KCN, and 50 μg of cell lysate. The reaction was initiated by the addition of 50 μM cytochrome *c*, and the increase in absorbance was monitored 1 min before and 1 min after the addition of 400 μM TTFA. Complex II-III activity was considered the TTFA-sensitive rate of succinate-induced cytochrome *c* reduction at 550 nm. Complex IV activity was measured using the cytochrome *c* oxidase assay kit supplied by Sigma. The Bradford assay was used to quantify the protein concentration.

Measurement of the NADH/NAD^+ ratio

To assess RET, the mitochondrial NADH/NAD^+ ratio was measured using the NAD^+/NADH quantification kit (BioVision) according to the manufacturer's instructions.

Western blot

Western blot was performed as described previously [16].

Statistical analysis

Results were expressed as means ± SE. Error bars represent the mean ± SE of at least three independent experiments. The difference between two mean values was analyzed using Student's *t*-test. The difference was considered statistically significant when $P < 0.05$.

Acknowledgments

We thank Tae Gyu Choi and Yeounghwan Kim for technical supports. This work has been supported by the Korea Science & Engineering Foundation (KOSEF) grant funded by the Korea government (MEST) (No. 20090091346) to SS Kim.

References

1 Facucho-Oliveira JM, Alderson J, Spikings EC, Egginton S, St John JC. Mitochondrial DNA replication during differentiation of murine embryonic stem cells. *J Cell Sci* 2007; **120**:4025-4034.

2 Lu J, Sharma LK, Bai Y. Implications of mitochondrial DNA mutations and mitochondrial dysfunction in tumorigenesis. *Cell Res* 2009; **19**:802-815.

3 Huang G, Chen Y, Lu H, Cao X. Coupling mitochondrial respiratory chain to cell death: an essential role of mitochondrial complex I in the interferon-beta and retinoic acid-induced cancer cell death. *Cell Death Differ* 2007; **14**:327-337.

4 Storz P, Döppler H, Toker A. Protein kinase D mediates mitochondrion-to-nucleus signaling and detoxification from mitochondrial reactive oxygen species. *Mol Cell Biol* 2005; **25**:8520-8530.

5 Murphy MP. How mitochondria produce reactive oxygen species. *Biochem J* 2009; **417:**1-13.

6 Bell EL, Klimova TA, Eisenbart J, *et al*. The Q_o site of the mitochondrial complex III is required for the transduction of hypoxic signaling via reactive oxygen species production. *J Cell Biol* 2007; **177**:1029-1036.

7 Lin MT, Beal MF. Mitochondrial dysfunction and oxidative stress in neurodegenerative diseases. *Nature* 2006; **443**:787-795.

8 Kaminski M, Kiessling M, Suss D, Krammer PH, Gulow K. Novel role for mitochondria: protein kinase C{theta}-dependent oxidative signaling organelles in activation-induced T-cell death. *Mol Cell Biol* 2007; **27**:3625-3639.
9 Oka S, Ohno M, Tsuchimoto D, Sakumi K, Furuichi M, Nakabeppu Y. Two distinct pathways of cell death triggered by oxidative damage to nuclear and mitochondrial DNAs. *EMBO J* 2008; **27**:421-432.
10 Cowell CF, Döppler H, Yan IK, Hausser A, Umezawa Y, Storz P. Mitochondrial diacylglycerol initiates protein-kinase D1-mediated ROS signaling. *J Cell Sci* 2009; **122**:919-928.
11 Benani A, Troy S, Carmona MC, *et al*. Role for mitochondrial reactive oxygen species in brain lipid sensing: Redox regulation of food intake. *Diabetes* 2007; **56**:152-160.
12 Hughes G, Murphy MP, Ledgerwood EC. Mitochondrial reactive oxygen species regulate the temporal activation of nuclear factor κB to modulate tumour necrosis factor-induced apoptosis: evidence from mitochondria-targeted antioxidants. *Biochem J* 2005; **389**:83-89.
13 Hoffman DL, Brookes PS. Oxygen sensitivity of mitochondrial reactive oxygen species generation depends on metabolic conditions. *J Biol Chem* 2009; **284**:16236-16245.
14 Forman HJ, Fukuto JM, Torres M. Redox signaling: thiol chemistry defines which reactive oxygen and nitrogen species can act as second messengers. *Am J Physiol Cell Physiol*. 2004; **287**:C246-C256.
15 Zelko IN, Mariani TJ, Folz RJ. Superoxide dismutase multigene family: a comparison of the CuZn-SOD (SOD1), Mn-SOD (SOD2), and EC-SOD (SOD3) gene structures, evolution, and expression. *Free Radic Biol Med* 2002; **33:**337–349.
16 Ding Y, Choi KJ, Kim JH, *et al*. Endogenous hydrogen peroxide regulates glutathione redox via nuclear factor erythroid 2-related factor 2 downstream of phosphatidylinositol 3-kinase during muscle differentiation. *Am J Pathol* 2008; **172**:1529-1541.
17 Lim MJ, Choi KJ, Ding Y, *et al*. RhoA/Rho kinase blocks muscle differentiation via serine phosphorylation of insulin receptor substrate-1 and -2. *Mol Endocrinol* 2007; **21**:2282-2293.
18 Lee J, Choi KJ, Lim MJ, *et al*. Proto-oncogenic H-Ras, K-Ras, and N-Ras are involved in muscle differentiation via phosphatidylinositol 3-kinase. *Cell Res* 2010; **20**:919-934.
19 Buggisch M, Ateghang B, Ruhe C, *et al*. Stimulation of ES-cell-derived cardiomyogenesis and neonatal cardiac cell proliferation by reactive oxygen species and NADPH oxidase. *J Cell Sci* 2007; **1**:885-894.
20 Piao YJ, Seo YH, Hong F, *et al*. Nox 2 stimulates muscle differentiation via NF-κB/iNOS pathway. *Free Radic Biol Med* 2005; **38**:989-1001.
21 Liochev SI, Fridovich I. The effects of superoxide dismutase on H_2O_2 formation. *Free Radic Biol Med* 2007; **42**:1465-1469.
22 Skaug B, Jiang X, Chen ZJ. The role of ubiquitin in NF-kappaB regulatory pathways. *Annu Rev Biochem* 2009; **78**:769-796.
23 Conejo R, Valverde AM, Benito M, Lorenzo M. Insulin produces myogenesis in C2C12 myoblasts by induction of NF-κB and downregulation of AP-1 activities. *J Cell Physiol* 2001; **186**:82-94.
24 De Alvaro C, Nieto-Vazquez I, Rojas JM, Lorenzo M. Nuclear exclusion of Forkhead Box O and Elk1 and activation of nuclear factor-κB are required for C2C12-RasV12C40 myoblast differentiation. *Endocrinology* **2008; 149**:793-801**.**
25 James AM, Sharpley MS, Manas AR, *et al*. Interaction of the mitochondria-targeted antioxidant MitoQ with phospholipid bilayers and ubiquinone oxidoreductases. *J Biol Chem* 2007; **282**:14708-14718.
26 Trnka J, Blaikie FH, Smith RA, Murphy MP. A mitochondria-targeted nitroxide is reduced to its hydroxylamine by ubiquinol in mitochondria. *Free Radic Biol Med* 2008; **44**:1406-1419.
27 Arita Y, Harkness SH, Kazzaz JA, *et al*. Mitochondrial localization of catalase provides optimal protection from H_2O_2-induced cell death in lung epithelial cells. *Am J Physiol Lung Cell Mol Physiol* 2006; **290**:L978-L986.
28 Franko A, Mayer S, Thiel G, *et al*. CREB-1alpha is recruited to and mediates upregulation of the cytochrome c promoter during enhanced mitochondrial biogenesis accompanying skeletal muscle differentiation. *Mol Cell Biol* 2008; **28**:2446-2459.
29 Wallace DC, Fan W. The pathophysiology of mitochondrial disease as modeled in the mouse. *Genes Dev* 2009; **23**:1714-1736.
30 Carroll J, Fearnley IM, Skehel JM, Shannon RJ, Hirst J, Walker JE. Bovine complex I is a complex of 45 different subunits. *J Biol Chem* 2006; **281**:32724-32427.
31 Vogel RO, Janssen RJ, van den Brand MA, *et al*. Cytosolic signaling protein Ecsit also localizes to mitochondria where it interacts with chaperone NDUFAF1 and functions in complex I assembly. *Genes Dev* 2007; **21**:615-624.
32 Vogel RO, Dieteren CE, van den Heuvel LP, Willems PH, Smeitink JA. Identification of mitochondrial complex I assembly intermediates by tracing tagged NDUFS3 demonstrates the entry point of mitochondrial subunits. *J Biol Chem* 2007; **282**:7582-7590.
33 Yudkoff M, Nelson D, Daikhin Y, Erecińska M. Tricarboxylic acid cycle in rat brain synaptosomes. Fluxes and interactions with aspartate aminotransferase and malate/aspartate shuttle. *J Biol Chem* 1994; **269**:27414-27420.
34 Panov A, Schonfeld P, Dikalov S, Hemendinger R, Bonkovsky HL, Brooks BR. The neuromediator glutamate, through specific substrate interactions, enhances mitochondrial ATP production and reactive oxygen species generation in non-synaptic brain mitochondria. *J Biol Chem* 2009; **284**:14448-14456.
35 Freedman JA, Lemasters JJ. Thermodynamics of reverse electron transfer across site 1: ATP/2e- is greater than one. *Biochem Biophys Res Commun* 1984; **125**:8-13.
36 Piantadosi CA, Suliman HB. Mitochondrial transcription factor A induction by redox activation of nuclear respiratory factor 1. *J Biol Chem* 2006; **281**:324-333.
37 Redout EM, Wagner MJ, Zuidwijk MJ, *et al*. Right-ventricular failure is associated with increased mitochondrial complex II activity and production of reactive oxygen species. *Cardiovasc Res* 2007; **75**:770-781.
38 Hoegger MJ, Lieven CJ, Levin LA. Differential production of superoxide by neuronal mitochondria. *BMC Neurosci* 2008; **9**:1-14.
39 Zhang DX, Gutterman DD. Mitochondrial reactive oxygen

species-mediated signaling in endothelial cells. *Am J Physiol Heart Circ Physiol* 2007; **292**:H2023-H2031.

40 Del Prete A, Zaccagnino P, Di Paola M, *et al*. Role of mitochondria and reactive oxygen species in dendritic cell differentiation and functions. *Free Radic Biol Med* 2008; **44**:1443-1451.

41 Habara-Ohkubo A. Differentiation of beating cardiac muscle cells from a derivative of P19 embryonal carcinoma cells. *Cell Struct Funct* 1996; **21**:101-110.

42 Choi KJ, Piao YJ, Lim MJ, *et al*. Overexpressed cyclophilin A in cancer cells renders resistance to hypoxia- and cisplatin-induced cell death. *Cancer Res* 2007; **67**:3654-3662.

43 Lambert AJ, Boysen HM, Buckingham JA, *et al*. Low rates of hydrogen peroxide production by isolated heart mitochondria associate with long maximum lifespan in vertebrate homeotherms. *Aging Cell* 2007; **6**:607-618.

44 Han HJ, Lim MJ, Lee YJ. Oxalate inhibits renal proximal tubule cell proliferation via oxidative stress, p38 MAPK/JNK, and cPLA2 signaling pathways. *Am J Physiol Cell Physiol* 2004; **287**:C1058-C1066.

45 Gao X, Campian JL, Qian M, Sun XF, Eaton JW. Mitochondrial DNA damage in iron overload. *J Biol Chem* 2009; **284**:4767-4775.

46 Kim J, Choi TG, Ding Y, *et al*. Overexpressed cyclophilin B suppresses apoptosis associated with ROS and Ca^{2+} homeostasis after ER stress. *J Cell Sci* 2008; **121**:3636-3648.

47 Reshkin SJ, Bellizzi A, Caldeira S, *et al*. Na+/H+ exchanger-dependent intracellular alkalinization is an early event in malignant transformation and plays an essential role in the development of subsequent transformation-associated phenotypes. *FASEB J* 2000; **14:**2185-2197.

48 Menna-Barreto RF, Goncalves RL, Costa EM, *et al*. The effects on Trypanosoma cruzi of novel synthetic naphthoquinones are mediated by mitochondrial dysfunction. *Free Radic Biol Med* 2009; **47**:644-653.